arXiv:1404.4302v1 [hep-ph] 16 Apr 2014

NNLO soft-gluon corrections for the Z-boson and W-boson transverse momentum distributions

Nikolaos Kidonakis[a] and Richard J. Gonsalves[b]

[a] *Kennesaw State University, Physics #1202, 1000 Chastain Rd., Kennesaw, GA 30144-5591, USA*

[b] *Department of Physics, University at Buffalo, The State University of New York, Buffalo, NY 14260-1500, USA*

Abstract

We present results for the Z-boson and W-boson transverse momentum (p_T) distributions for large p_T at LHC and Tevatron energies. We calculate complete next-to-leading-order (NLO) QCD corrections as well as soft-gluon corrections at next-to-next-to-leading-order (NNLO) to the differential cross section. The NNLO soft-gluon contributions are derived from next-to-next-to-leading-logarithm (NNLL) resummation at two loops. We find enhancements of the p_T distributions and reductions of the scale dependence when the NNLO corrections are included.

1 Introduction

The production of Z and W bosons with large transverse momentum, p_T, has been observed and analyzed at both the Tevatron [1, 2] and the LHC [3, 4]. The study of electroweak boson production complements studies of Higgs physics and top quark production in the Standard Model. Furthermore, these processes are backgrounds to new physics that may be within reach of the LHC, and thus it is important to have precise theoretical predictions. High-p_T W production has a clean experimental signature when an on-shell W decays to leptons, and accurate predictions are needed to reduce uncertainties in precision measurements of the W mass and decay width. The charged leptons in complementary processes involving Z bosons can be measured with somewhat higher resolution than the neutrino, but the observed event rate for W bosons at the LHC is larger than that for Z bosons produced on shell. The event rate for the underlying production mechanism is enhanced experimentally by measuring off-shell Z bosons and virtual photons decaying to lepton pairs.

At leading order (LO) in the strong coupling, α_s, an electroweak boson can be produced with large p_T by recoiling against a single parton which decays into a jet of hadrons. The LO partonic processes for Z production at large p_T are $qg \to Zq$ and $q\bar{q} \to Zg$, and for W production they are $qg \to Wq'$ and $q\bar{q}' \to Wg$. The next-to-leading-order (NLO) corrections, involving virtual one-loop graphs and two-parton final states, for Z and W production at large p_T were calculated in [5, 6] where complete analytic expressions were provided. The NLO corrections enhance the differential p_T distributions and they reduce the factorization and renormalization scale dependence.

Higher-order contributions to electroweak-boson production from the emission of soft gluons have also been calculated. These corrections appear in the form of logarithms which can be

formally resummed, and they were first calculated to next-to-leading-logarithm (NLL) accuracy in [7] using the moment-space resummation formalism in perturbative Quantum ChromoDynamics (pQCD). Approximate next-to-next-to-leading-order (NNLO) corrections derived from the resummation were calculated in [8] and were shown to provide enhancements and a further reduction of the scale dependence. Numerical results for the W-boson p_T distribution were presented for 1.8 and 1.96 TeV energies at the Tevatron in [8] and for 14 TeV energy at the LHC in Ref. [9]. With the calculation of two-loop soft-anomalous dimensions [10, 11], the resummation was extended to next-to-next-to-leading-logarithm (NNLL) accuracy in [11]. Exact NLO results and approximate NNLO results from NNLL resummation for the W-boson p_T distribution were presented at 1.96 TeV energy at the Tevatron and at 7, 8, and 14 TeV energies at the LHC in [11] (see also [12]).

In addition to the moment-space pQCD resummation work described above, related theoretical and numerical studies for electroweak-boson production using resummation in Soft-Collinear Effective Theory (SCET) have appeared in [13, 14, 15, 16].

In this paper we present the first results for Z production at approximate NNLO using the pQCD moment-space NNLL resummation formalism, and we show the p_T distribution of the Z boson at 1.96 TeV Tevatron energy and at 7, 8, 13, and 14 TeV LHC energies. We also present corresponding results for the W-boson p_T distribution, thus extending and updating our previously published results on W production. We find in general that the approximate NNLO distributions are reliably estimated at fixed order α_s^3 over the experimentally accessible phase space with $p_T \geq 20$ GeV.

In the next section we give some details of the analytical calculation. Section 3 presents numerical results at Tevatron and LHC energies for the Z-boson p_T distribution. Section 4 has the corresponding results for the W-boson p_T distribution. We conclude in Section 5.

2 Analytical results

We start with the LO contributions to electroweak boson production at large p_T with a single hard parton in the final state. The two contributing sub-processes for Z production are (see Fig. 1)

$$q(p_a) + g(p_b) \longrightarrow Z(Q) + q(p_c)$$

and

$$q(p_a) + \bar{q}(p_b) \longrightarrow Z(Q) + g(p_c)$$

and similarly for W production. We define the kinematic variables $s = (p_a + p_b)^2$, $t = (p_a - Q)^2$, $u = (p_b - Q)^2$, and note that $p_T^2 = tu/s$. We also define the threshold variable $s_4 = s + t + u - Q^2$. As we approach partonic threshold, where there is no available energy for additional radiation, $s_4 \to 0$.

The LO differential cross section for the $qg \to Zq$ process is

$$E_Q \frac{d\sigma^B_{qg\to Zq}}{d^3Q} = F^B_{qg\to Zq}\, \delta(s_4)\,, \tag{2.1}$$

with

$$F^B_{qg\to Zq} = \frac{\alpha\, \alpha_s(\mu_R^2) C_F}{s(N_c^2 - 1)} A^{qg}\, |L^Z_{qg}|^2\,, \tag{2.2}$$

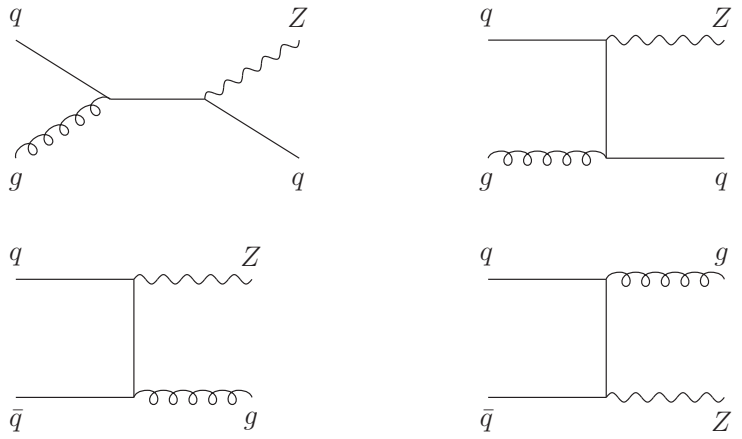

Figure 1: LO diagrams for the processes $qg \to Zq$ (top two graphs) and $q\bar{q} \to Zg$ (bottom two graphs).

$$A^{qg} = -\left(\frac{s}{t} + \frac{t}{s} + \frac{2m_Z^2 u}{st}\right), \tag{2.3}$$

$$|L_{dg}^Z|^2 = \frac{4\sin^4\theta_W - 6\sin^2\theta_W + \frac{9}{2}}{18\sin^2\theta_W\cos^2\theta_W} \tag{2.4}$$

for $q = d$ (or s or b) quark, and

$$|L_{ug}^Z|^2 = \frac{16\sin^4\theta_W - 12\sin^2\theta_W + \frac{9}{2}}{18\sin^2\theta_W\cos^2\theta_W} \tag{2.5}$$

for $q = u$ (or c or t) quark, where $\alpha = e^2/4\pi$, α_s is the strong coupling, μ_R is the renormalization scale, m_Z is the Z-boson mass, θ_W is the weak mixing angle, and $C_F = (N_c^2 - 1)/(2N_c)$ with $N_c = 3$ the number of colors.

For the process $q\bar{q} \to Zg$ the LO result is

$$E_Q \frac{d\sigma^B_{q\bar{q}\to Zg}}{d^3Q} = F^B_{q\bar{q}\to Zg}\,\delta(s_4)\,, \tag{2.6}$$

with

$$F^B_{q\bar{q}\to Zg} = \frac{\alpha\,\alpha_s(\mu_R^2)C_F}{sN_c} A^{q\bar{q}}\,|L^Z_{q\bar{q}}|^2\,, \tag{2.7}$$

$$A^{q\bar{q}} = \frac{t}{u} + \frac{u}{t} + \frac{2m_Z^2 s}{tu}\,, \tag{2.8}$$

with $|L^Z_{d\bar{d}}| = |L^Z_{dg}|$ and $|L^Z_{u\bar{u}}| = |L^Z_{ug}|$.

For W production the results are very similar and can be obtained from the above equations with the changes $Z \to W$, $m_Z \to m_W$, and $|L^W_{qg}| = |L^W_{q\bar{q}'}| = V_{qq'}/(\sqrt{2}\sin\theta_W)$ with $V_{qq'}$ the CKM matrix elements.

The NLO corrections arise from one-loop parton processes with a virtual gluon, and real radiative processes with two partons in the final state. The complete NLO corrections were derived in [5, 6]. They may be written as

$$E_Q \frac{d\sigma^{(1)}_{f_a f_b \to ZX}}{d^3Q} = \alpha_s^2(\mu_R^2) \left[\delta(s_4)\, B(s,t,u,\mu_R) + C(s,t,u,s_4,\mu_F)\right] \tag{2.9}$$

where μ_F is the factorization scale and X denotes additional final-state particles. The coefficient functions B and C depend on the partons f_a, f_b in the initial state. The coefficient $B(s,t,u,\mu_R)$ is the sum of virtual corrections and of singular terms proportional to $\delta(s_4)$ in the real radiative corrections. Coefficient $C(s,t,u,s_4,\mu_F)$ represents real emission processes away from $s_4 = 0$.

An important subset of the NLO corrections are those from soft-gluon emission. We can write the NLO soft and virtual (S+V) corrections for the partonic processes for Z production as

$$E_Q \frac{d\sigma^{(1)\,\mathrm{S+V}}_{f_a f_b \to ZX}}{d^3Q} = F^B_{f_a f_b \to ZX} \frac{\alpha_s(\mu_R^2)}{\pi} \left\{ c_3^{f_a f_b} \left[\frac{\ln(s_4/p_T^2)}{s_4}\right]_+ + c_2^{f_a f_b} \left[\frac{1}{s_4}\right]_+ + c_1^{f_a f_b}\, \delta(s_4) \right\} \tag{2.10}$$

and similarly for W production. The coefficients c_3 and c_2 of the plus-distribution terms in Eq. (2.10) can be derived from soft-gluon resummation, and their expressions are the same for Z and W production. The leading-logarithm coefficient, c_3, depends only on the identities of the incoming partons, but c_2 also depends on the details of the partonic process. These coefficients are given by $c_3^{qg} = C_F + 2C_A$ and $c_3^{q\bar{q}} = 4C_F - C_A$; $c_2^{qg} = -(C_F + C_A)\ln(\mu_F^2/p_T^2) - 3C_F/4$ and $c_2^{q\bar{q}} = -2C_F \ln(\mu_F^2/p_T^2) - \beta_0/4$, where $C_A = N_c$ and $\beta_0 = (11C_A - 2n_f)/3$ is the lowest-order term in the QCD beta function with $n_f = 5$ the number of light-quark flavors. The coefficients of the $\delta(s_4)$ terms are given by

$$c_1^{qg} = \frac{1}{2A^{qg}} \left[B_1^{qg} + B_2^{qg} n_f + C_1^{qg} + C_2^{qg} n_f\right] - \frac{c_3^{qg}}{2} \ln^2\left(\frac{p_T^2}{Q^2}\right) + c_2^{qg} \ln\left(\frac{p_T^2}{Q^2}\right), \tag{2.11}$$

and

$$c_1^{q\bar{q}} = \frac{1}{2A^{q\bar{q}}} \left[B_1^{q\bar{q}} + C_1^{q\bar{q}} + (B_2^{q\bar{q}} + D_{aa}^{(0)})\, n_f\right] - \frac{c_3^{q\bar{q}}}{2} \ln^2\left(\frac{p_T^2}{Q^2}\right) + c_2^{q\bar{q}} \ln\left(\frac{p_T^2}{Q^2}\right), \tag{2.12}$$

with B_1, B_2, C_1, C_2, and $D^{(0)}$ as given in the Appendix of the first paper in Ref. [6] but without the renormalization counterterms and using $f_A \equiv \ln(A/Q^2) = 0$ [note that the terms not multiplying A^{qg} in Eq. (A4) for B_1^{qg} of Ref. [6] should have the opposite sign than shown in that paper]. Note that Eqs. (2.11) and (2.12) correct the sign of the next-to-last term in Eqs. (4.3) and (4.10) of Ref. [11]. This correction also affects the approximate NNLO numerical results in [11].

As we will show in the next section, the soft-gluon corrections are numerically important. These corrections can be formally resummed in moment space at NNLL accuracy via the use of two-loop soft anomalous dimensions, the calculation of which involves two-loop diagrams in the eikonal approximation [10, 11]. The resummed cross section can then be used as a generator of NNLO approximate corrections [11].

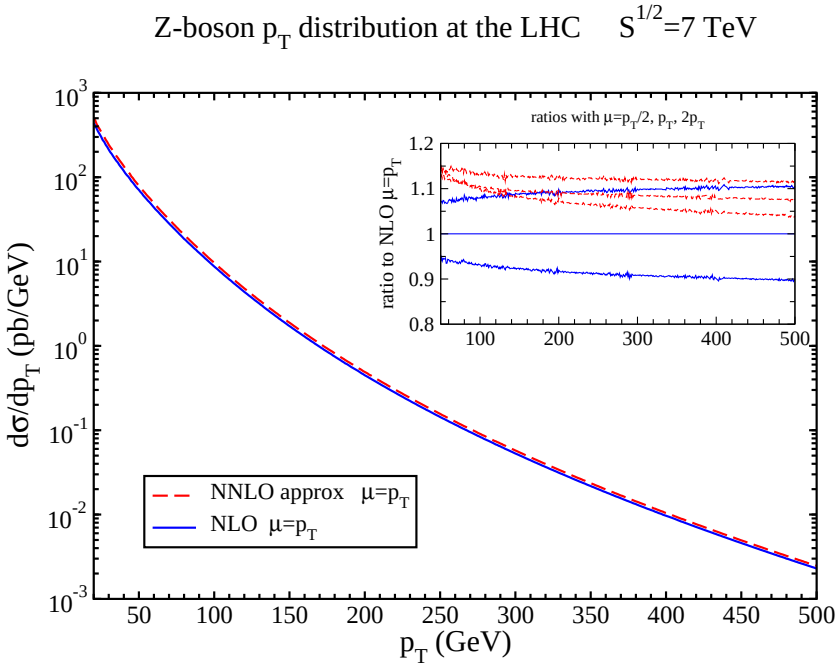

Figure 2: Z-boson p_T distribution at the LHC at 7 TeV energy.

The NNLO expansion of the resummed cross section involves logarithms $\ln^k(s_4/p_T^2)$ with $k = 0, 1, 2, 3$. At NNLL accuracy the coefficients of all these logarithmic terms can be fully determined, and explicit expressions were already provided in Ref. [11] for W production; the analytical results are identical for Z production and will not be repeated here. In addition, the $\delta(s_4)$ terms involving the factorization and renormalization scales have also been calculated at NNLO [8]. We denote the sum of the exact NLO cross section and the soft-gluon NNLO corrections as "approximate NNLO." We will employ the above results, with the noted corrections, to study the Z-boson and W-boson large-p_T distributions for various collider energies, $\sqrt{S}$, at the LHC and the Tevatron.

3 Z-boson production

In this section we present numerical results for the p_T distribution of the Z boson in pp collisions at the LHC with $\sqrt{S} = 7$, 8, 13, and 14 TeV and in $p\bar{p}$ collisions at the Tevatron with $\sqrt{S} = 1.96$ TeV. We use the MSTW2008 [17] parton distribution functions (pdf). We consistently use NLO pdf for the NLO results and NNLO pdf for the approximate NNLO results.

We begin with results for Z production at the LHC at 7 TeV energy. In Fig. 2 we plot the Z-boson p_T distribution, $d\sigma/dp_T$, for p_T values up to 500 GeV. We compare the exact NLO and the approximate NNLO results at 7 TeV LHC energy with central scale $\mu = p_T$. The p_T distribution spans six orders of magnitude in the range of p_T shown in the figure. The inset plot shows the ratios of the NLO and approximate NNLO results with different scales, $\mu = p_T/2$, p_T, $2p_T$ to the NLO central result with $\mu = p_T$. The approximate NNLO corrrections provide

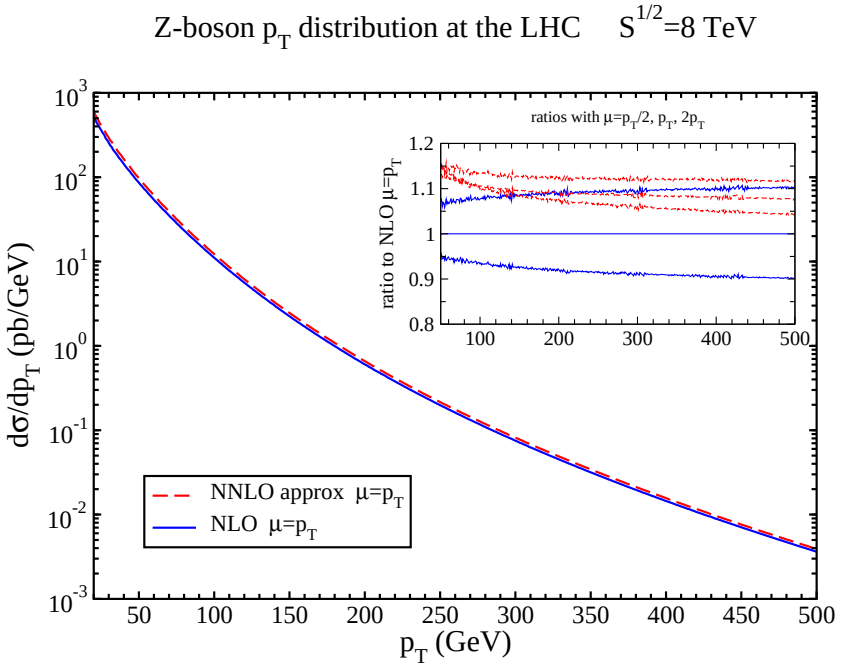

Figure 3: Z-boson p_T distribution at the LHC at 8 TeV energy.

an increase of the NLO central result, of the order of 10% for $\mu = p_T$ (the increase varies from ∼13% at $p_T = 50$ GeV to ∼8% at $p_T = 500$ GeV). It is also seen that the scale dependence at approximate NNLO is significantly smaller than at NLO, so there is a decrease in the theoretical uncertainty over all p_T values shown. While at NLO the scale variation is around ±10%, at approximate NNLO it is only at most a few percent.

We continue with results for Z production at the LHC at 8 TeV energy. In Fig. 3 we again show the Z-boson p_T distribution at NLO and approximate NNLO. The inset plot again shows ratios with different scales. Although the overall values for $d\sigma/dp_T$ are higher for this larger energy, the ratios in the inset plots are very similar at 7 and 8 TeV energies.

In Fig. 4 we show the corresponding results at 13 TeV LHC energy and the p_T range shown is up to 1000 GeV. Again, the approximate NNLO corrections enhance the cross section (from ∼14% at $p_T = 50$ GeV to ∼7% at $p_T = 1000$ GeV, for $\mu = p_T$) while reducing the scale dependence.

Figure 5 shows the Z-boson p_T distribution for 14 TeV energy at the LHC. The distribution falls over seven orders of magnitude in the p_T range shown. The scale ratios and the overall enhancement from the soft-gluon NNLO corrections at 14 TeV are very similar to those at 13 TeV.

Finally, in Fig. 6 we show the Z-boson p_T distribution at the Tevatron energy of 1.96 TeV for a p_T up to 350 GeV. The inset plot again displays the reduction in scale dependence from around ±10% at NLO to a few percent when the approximate NNLO corrections are included. The enhancement from these corrections varies from ∼10% at $p_T = 50$ GeV to ∼4% at $p_T = 350$ GeV, for $\mu = p_T$.

It is important to check how well the soft-gluon approximation works. In Fig. 7 we plot

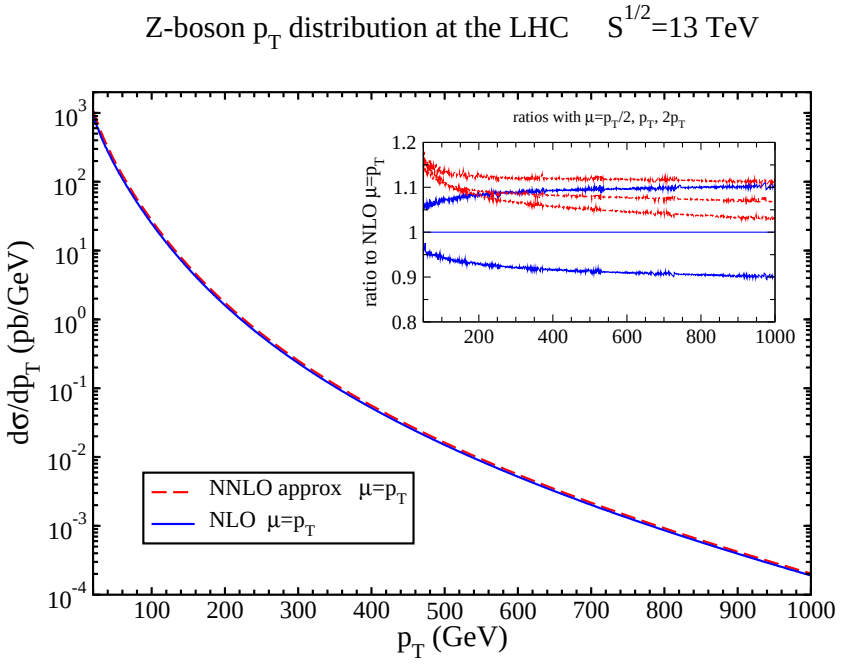

Figure 4: Z-boson p_T distribution at the LHC at 13 TeV energy.

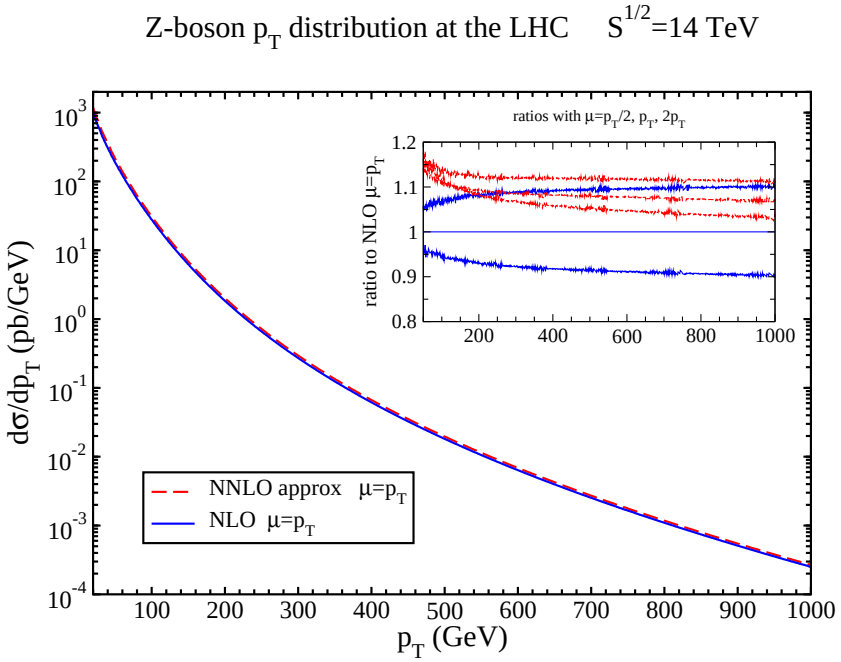

Figure 5: Z-boson p_T distribution at the LHC at 14 TeV energy.

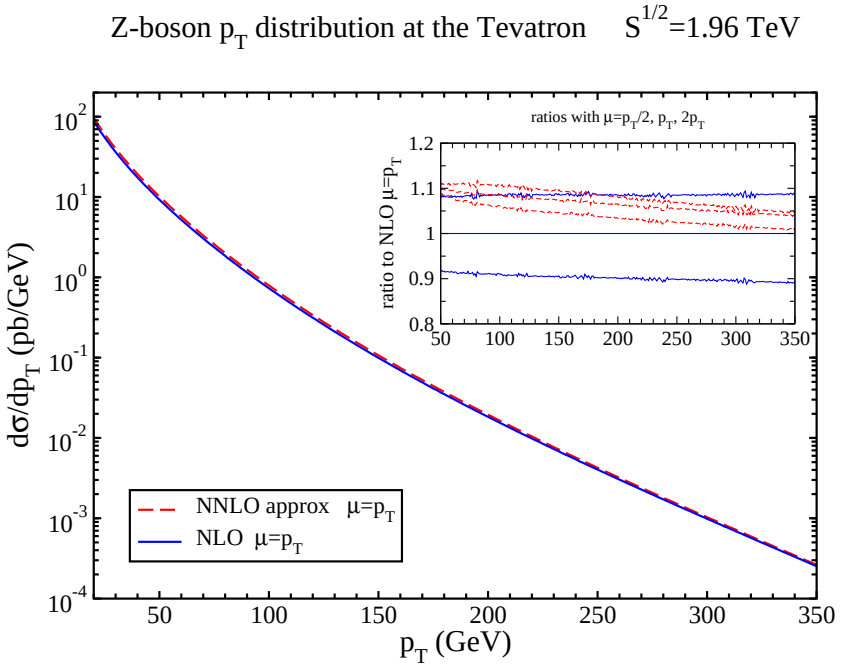

Figure 6: Z-boson p_T distribution at the Tevatron at 1.96 TeV energy.

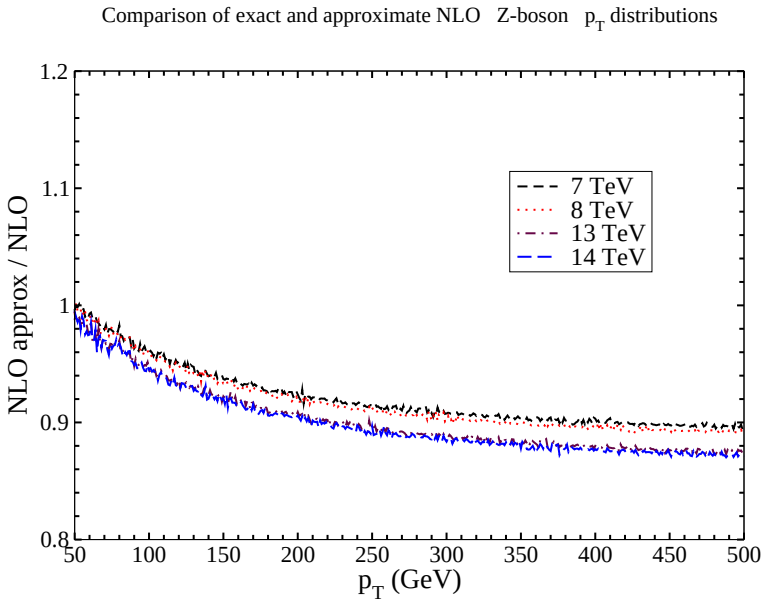

Figure 7: Comparison of the approximate and exact NLO Z-boson p_T distributions at LHC energies. The 7 and 8 TeV curves (upper two lines) are very similar, as are the 13 and 14 TeV curves (lower two lines).

Z boson	$\sigma(100\text{ GeV} \leq p_T \leq p_T^{\rm up})$		$\sigma(200\text{ GeV} \leq p_T \leq p_T^{\rm up})$	
$\sqrt{S}$	NLO	NNLO approx	NLO	NNLO approx
LHC 7 TeV	277^{+24}_{-20}	305^{+8}_{-4}	$20.7^{+2.0}_{-1.8}$	$22.5^{+0.8}_{-0.5}$
LHC 8 TeV	360^{+29}_{-26}	395^{+11}_{-3}	$28.6^{+2.7}_{-2.4}$	$31.1^{+1.0}_{-0.6}$
LHC 13 TeV	863^{+66}_{-54}	951^{+24}_{-3}	$84.0^{+7.2}_{-6.4}$	$91.4^{+2.8}_{-1.3}$
LHC 14 TeV	979^{+72}_{-61}	1078^{+28}_{-2}	$97.6^{+8.3}_{-7.3}$	$106.2^{+3.2}_{-1.5}$
Tevatron 1.96 TeV	$18.3^{+1.6}_{-1.7}$	$19.8^{+0.4}_{-0.5}$	$0.602^{+0.051}_{-0.061}$	$0.637^{+0.009}_{-0.018}$

Table 1: NLO and approximate NNLO Z-boson cross sections, in pb, integrated over p_T from 100 or 200 GeV to an upper value $p_T^{\rm up}$ which is 350 GeV at the Tevatron, 500 GeV at 7 and 8 TeV LHC energy, and 1000 GeV at 13 and 14 TeV LHC energy. The indicated uncertainty is from scale variation between $p_T/2$ and $2p_T$.

the ratio of the NLO approximate (Eq. (2.10)) over the NLO exact (Eq. (2.9)) Z-boson p_T distributions at LHC energies. We see that the approximation is very good, with the approximate NLO results being 90% to 100% of the full NLO results, depending on the p_T value and the collider energy. At the Tevatron, kinematically closer to threshold, the approximation is even better with the approximate NLO result being 96% to 100% of the full NLO value. These results give confidence that the NNLO soft-gluon corrections capture the majority of NNLO contributions and that the approximate NNLO results in Figs. 2-6 are close to the (yet unknown) exact NNLO quantities.

In addition to scale variation another source of uncertainty comes from the parton distribution function sets used. In Fig. 8 we compare the scale and pdf uncertainties (using MSTW2008 NNLO 90% CL pdf sets [17]) at approximate NNLO for Z-boson p_T distributions at Tevatron and LHC energies. We show ratios relative to the approximate NNLO central set with $\mu = p_T$. The scale variation is again with μ ranging from $p_T/2$ to $2p_T$. At the Tevatron the pdf uncertainty is larger than the scale variation for all p_T values shown, especially at higher p_T. At LHC energies the pdf uncertainty is somewhat smaller than scale variation for most of the p_T range. Both pdf uncertainties and scale variation are a few percent.

In Table 1 we present integrated p_T distributions in two representative p_T bins at the highest experimentally accessible values. Cross section values in picobarns are given for exact fixed-order NLO and enhanced approximate NNLO predictions along with scale uncertainties. The enhancement from the NNLO soft-gluon corrections over NLO is around 10% for all four LHC energies, and around 8% at the Tevatron, when integrated over p_T higher than 100 GeV. The scale variation is reduced significantly, by factors of three or four, with the inclusion of these NNLO corrections. These results would appear to indicate that the predicted event rates are reliably estimated at approximate NNLO. Deviations from these predicted values would very likely indicate new physics beyond the Standard Model.

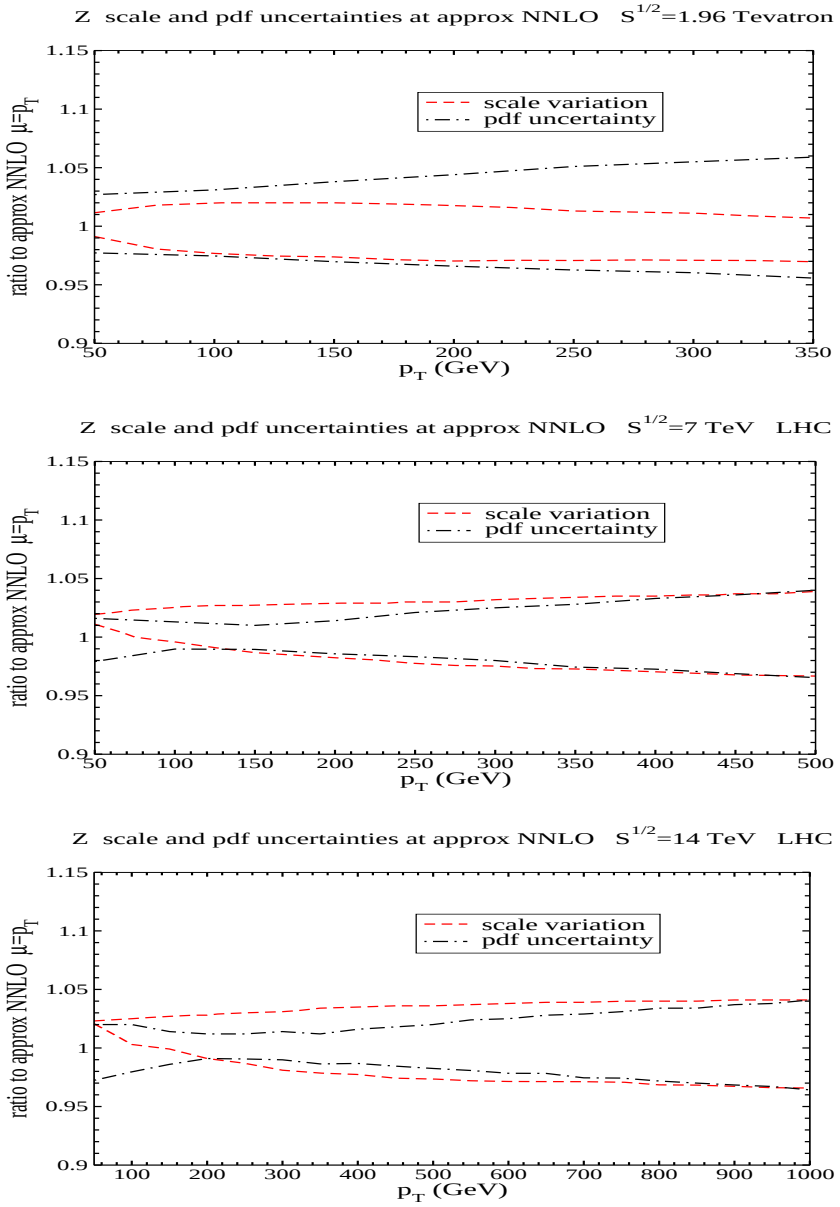
Z scale and pdf uncertainties at approx NNLO S^1/2=1.96 Tevatron
scale variation
pdf uncertainty
ratio to approx NNLO μ=p_T
p_T (GeV)
Z scale and pdf uncertainties at approx NNLO S^1/2=7 TeV LHC
scale variation
pdf uncertainty
ratio to approx NNLO μ=p_T
p_T (GeV)
Z scale and pdf uncertainties at approx NNLO S^1/2=14 TeV LHC
scale variation
pdf uncertainty
ratio to approx NNLO μ=p_T
p_T (GeV)

Figure 8: Comparison of the scale and pdf uncertainties at approximate NNLO for Z-boson p_T distributions at Tevatron energy (upper plot) and at LHC energies of 7 TeV (middle plot) and 14 TeV (lower plot). The upper (lower) scale line in each plot is for $\mu = p_T/2$ ($2p_T$).

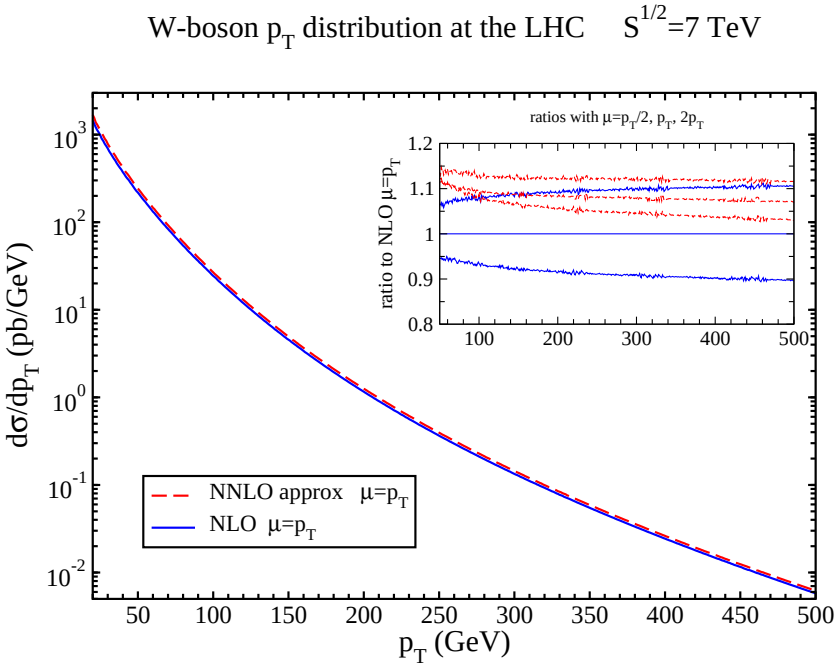

Figure 9: W-boson p_T distribution at the LHC at 7 TeV energy.

4 W-boson production

In this section we present corresponding numerical results for W-boson production. All results are for the sum of W^+ and W^- differential cross sections.

We begin with results for W production at the LHC at 7 TeV energy. In Fig. 9 we plot the W-boson p_T distribution, $d\sigma/dp_T$, for p_T values up to 500 GeV. We compare the NLO and the approximate NNLO results with $\mu = p_T$. The inset plot shows the ratios of the NLO and approximate NNLO results with different scales, $\mu = p_T/2$, p_T, $2p_T$ to the NLO result with $\mu = p_T$. The scale dependence at approximate NNLO is significantly smaller than at NLO, and the approximate NNLO corrrections provide an increase of the NLO central result with a decrease in the theoretical uncertainty over all p_T values shown. The results are similar to the corresponding ones for Z production shown in the previous section, except that the overall rate is higher for W production.

We continue with results for W production at the LHC at 8 TeV energy. In Fig. 10 we again show the W-boson p_T distribution at NLO and approximate NNLO. The inset plot shows ratios of the distributions with different scales. Again, the ratios in the inset plots are very similar at 7 and 8 TeV energies. The approximate NNLO corrections enhance the cross section (from $\sim$11% at $p_T = 50$ GeV to $\sim$7% at $p_T = 500$ GeV, for $\mu = p_T$) while reducing the scale dependence.

In Fig. 11 we show the corresponding results for the W-boson p_T distribution at 13 TeV LHC energy and the p_T range shown is up to 1000 GeV. Again, the approximate NNLO corrections enhance the cross section while significantly reducing the scale dependence.

In Fig. 12 we show the W-boson p_T distribution for 14 TeV energy at the LHC. The scale

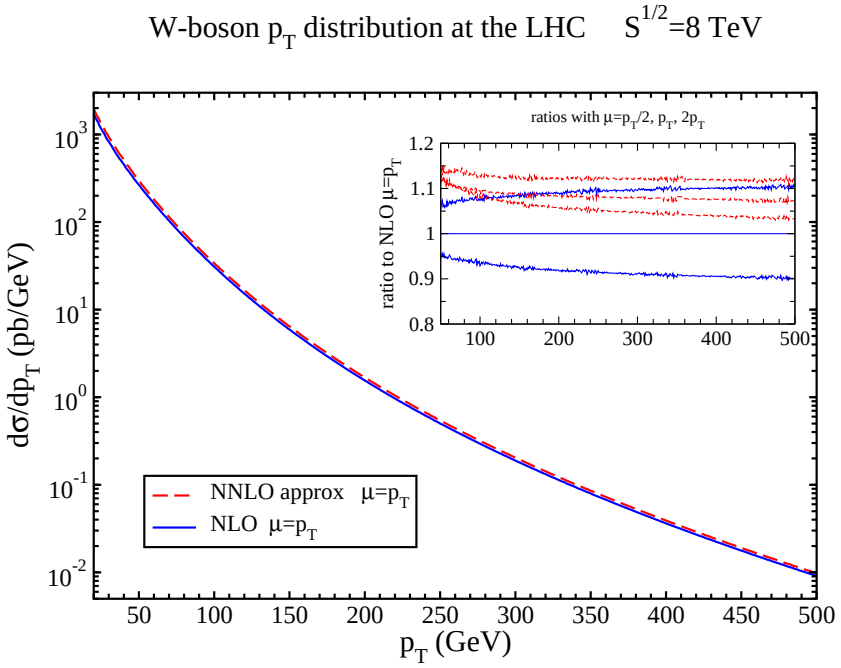

Figure 10: W-boson p_T distribution at the LHC at 8 TeV energy.

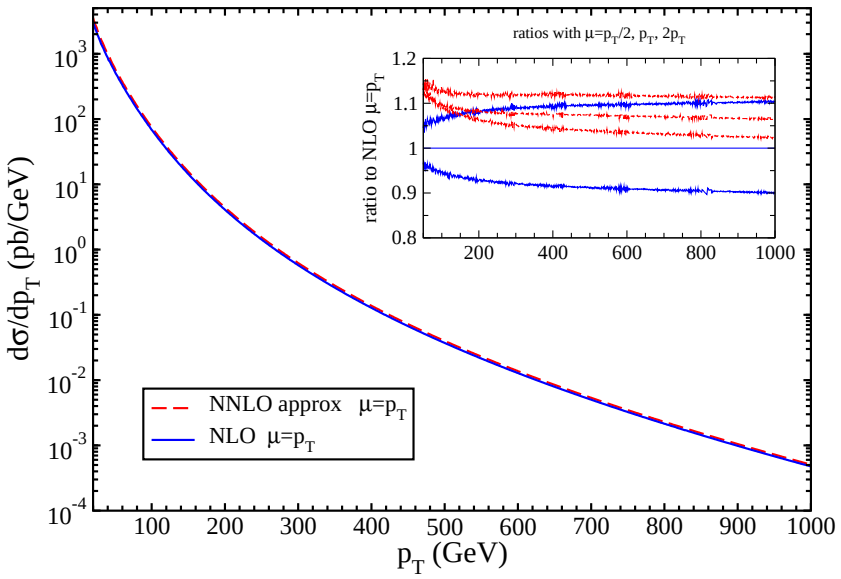

Figure 11: W-boson p_T distribution at the LHC at 13 TeV energy.

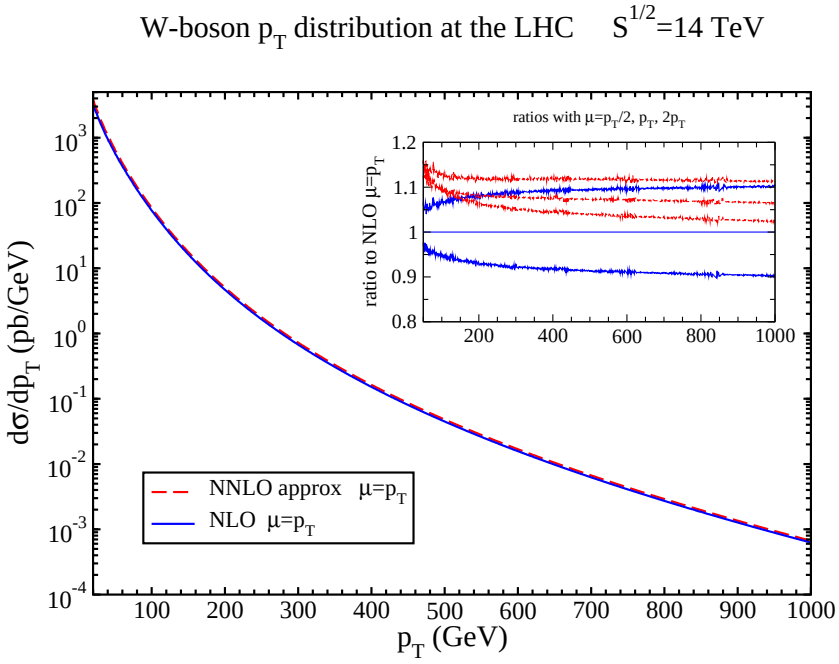

Figure 12: W-boson p_T distribution at the LHC at 14 TeV energy.

ratios at 14 TeV are very similar to those at 13 TeV. The approximate NNLO corrections enhance the cross section (from ∼12% at $p_T = 50$ GeV to ∼7% at $p_T = 1000$ GeV, for $\mu = p_T$) while reducing the scale dependence. These ratios are also similar to the corresponding ones for the Z boson.

Finally, in Fig. 13 we show the W-boson p_T distribution for the Tevatron energy of 1.96 TeV for p_T values up to 350 GeV. The inset plot again displays the enhancement from the approximate NNLO corrections (from ∼10% at $p_T = 50$ GeV to ∼5% at $p_T = 350$ GeV, for $\mu = p_T$) and the reduction in scale dependence.

In Fig. 14 we compare the scale and pdf uncertainties at approximate NNLO for the W-boson p_T distributions at Tevatron and LHC energies. Again at the Tevatron the pdf uncertainty is higher than scale variation while at LHC energies the scale variation is larger than the pdf uncertainties for most p_T values. These results are very similar to those for the Z boson in the previous section.

In Table 2 we present results for integrated high-p_T W-boson distributions for the same set of parameter values as in Table 1 for Z-boson production. Once again we note that these rates indicate similar progressive enhancement from NLO to NNLO with significant reduction in scale uncertainty. These results indicate that the pQCD predictions for the event rates in these highest p_T bins are reliable for both Z and W production at the Tevatron and the LHC. The integrated cross sections in the higher bin with $p_T \geq 200$ GeV for both W and Z production at the Tevatron and the LHC are compatible with corresponding $\text{NNLO}_{\text{sing}}$ + NLO results presented in Table 1 of [13] and Table 2 of [16] using the SCET formalism. Our results display a somewhat larger enhancement from NNLO soft-gluon corrections and a smaller scale uncertainty than the corresponding ones in [13, 16].

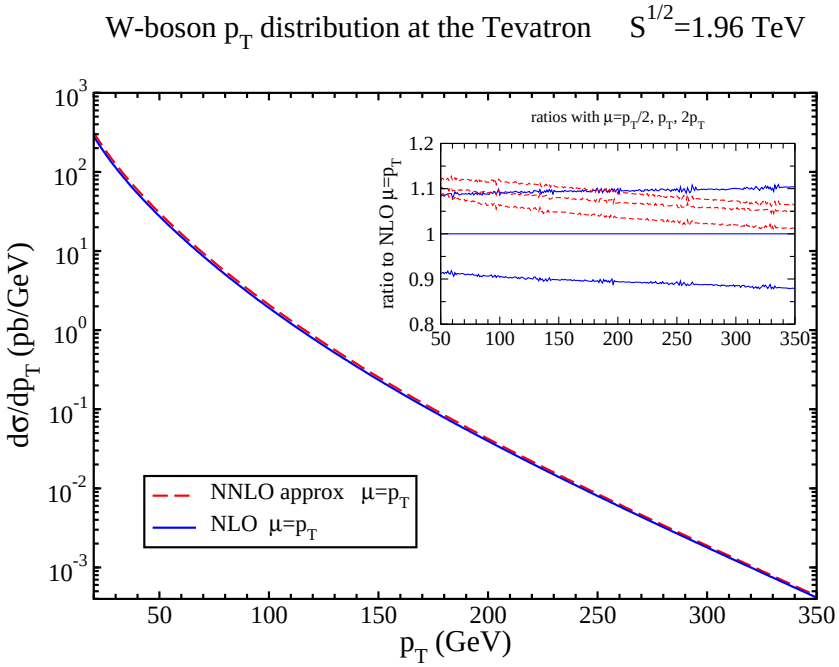

Figure 13: W-boson p_T distribution at the Tevatron at 1.96 TeV energy.

W boson	$\sigma(100\text{ GeV} \leq p_T \leq p_T^{\rm up})$		$\sigma(200\text{ GeV} \leq p_T \leq p_T^{\rm up})$	
$\sqrt{S}$	NLO	NNLO approx	NLO	NNLO approx
LHC 7 TeV	749^{+63}_{-56}	816^{+27}_{-14}	$52.8^{+5.1}_{-4.6}$	$57.1^{+2.2}_{-1.6}$
LHC 8 TeV	967^{+80}_{-69}	1054^{+35}_{-17}	$72.7^{+6.8}_{-6.2}$	$78.6^{+2.9}_{-2.2}$
LHC 13 TeV	2297^{+167}_{-143}	2502^{+77}_{-23}	211^{+18}_{-16}	227^{+9}_{-5}
LHC 14 TeV	2599^{+188}_{-156}	2831^{+88}_{-23}	245^{+20}_{-19}	264^{+10}_{-6}
Tevatron 1.96 TeV	$45.4^{+4.2}_{-4.5}$	$49.3^{+1.1}_{-1.4}$	$1.23^{+0.12}_{-0.13}$	$1.31^{+0.03}_{-0.04}$

Table 2: NLO and approximate NNLO W-boson cross sections, in pb, integrated over p_T from 100 or 200 GeV to an upper value $p_T^{\rm up}$ which is 350 GeV at the Tevatron, 500 GeV at 7 and 8 TeV LHC energy, and 1000 GeV at 13 and 14 TeV LHC energy. The uncertainty is from scale variation between $p_T/2$ and $2p_T$.

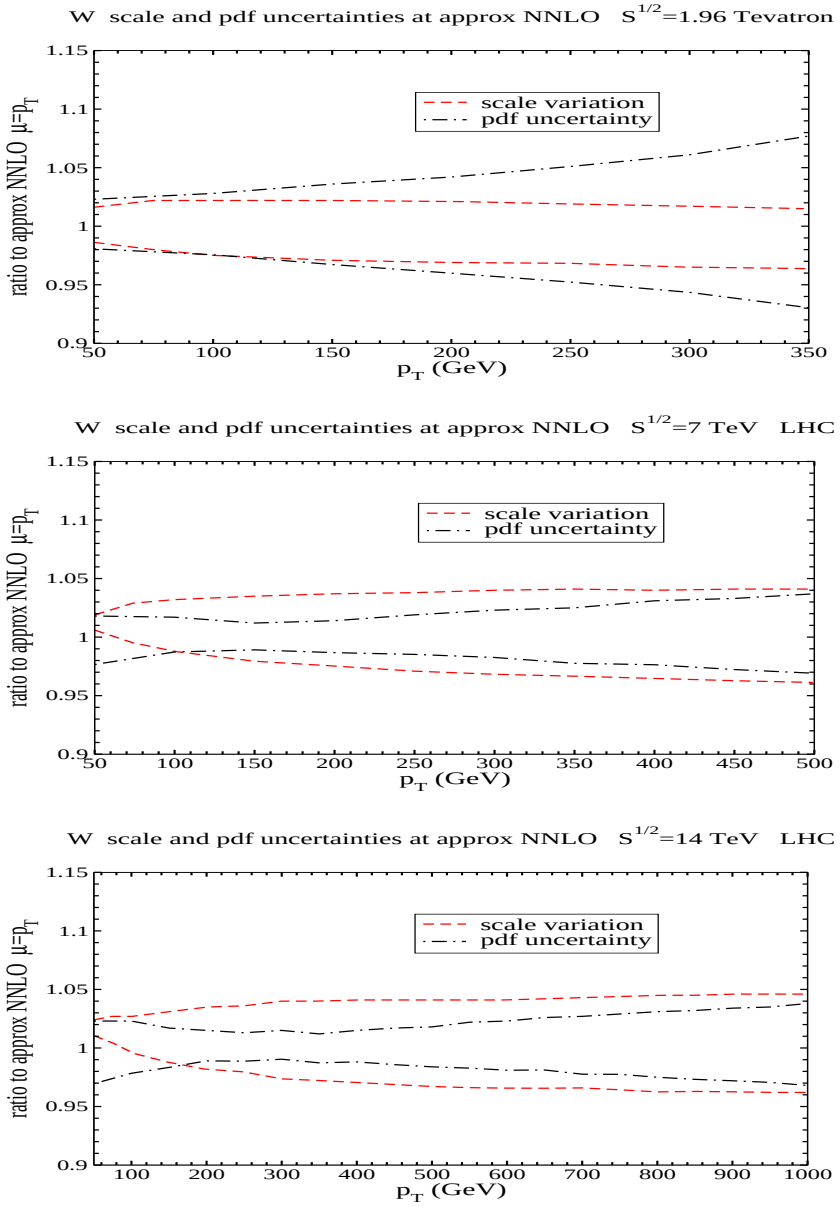
W scale and pdf uncertainties at approx NNLO S^1/2=1.96 Tevatron
ratio to approx NNLO μ=p_T
scale variation
pdf uncertainty
p_T (GeV)
W scale and pdf uncertainties at approx NNLO S^1/2=7 TeV LHC
ratio to approx NNLO μ=p_T
scale variation
pdf uncertainty
p_T (GeV)
W scale and pdf uncertainties at approx NNLO S^1/2=14 TeV LHC
ratio to approx NNLO μ=p_T
scale variation
pdf uncertainty
p_T (GeV)

Figure 14: Comparison of the scale and pdf uncertainties at approximate NNLO for W-boson p_T distributions at Tevatron energy (upper plot) and at LHC energies of 7 TeV (middle plot) and 14 TeV (lower plot). The upper (lower) scale line in each plot is for $\mu = p_T/2$ ($2p_T$).

5 Conclusions

In this paper we have presented theoretical perturbative QCD predictions for both Z-boson and W-boson differential cross sections at large p_T at NLO and approximate NNLO at the Tevatron and the LHC. The NNLO soft-gluon corrections increase rates and decrease dependence on renormalization and factorization scales. The magnitudes of these effects and the general trends from LO through approximate NNLO indicate that the perturbation series is reliably under control. Since we have shown that at NLO most of the corrections are from soft-gluon emission, it is very likely that the approximate NNLO corrections provide a reliable estimate of the as yet uncomputed complete fixed-order α_s^3 corrections. Our results indicate that it is likely not necessary to add even higher-order soft-gluon effects, beyond the NNLO corrections computed in this paper, in these inclusive p_T distributions at experimentally accessible energies. These conclusions should also hold true in comparing these QCD predictions to the fiducial cross sections measured experimentally with phase space cuts on the invariant mass, transverse momenta and rapidities of the lepton pairs.

Acknowledgements

The work of N.K. was supported by the National Science Foundation under Grant No. PHY 1212472.

References

[1] CDF Collaboration, F. Abe *et al.*, Phys. Rev. Lett. **66**, 2951 (1991).

[2] D0 Collaboration, B. Abbott *et al.*, Phys. Rev. Lett. **80**, 5498 (1998) [hep-ex/9803003]; V.M. Abazov *et al.*, Phys. Lett. B **513**, 292 (2001) [hep-ex/0010026]; Phys. Rev. Lett. **100**, 102002 (2008) [arXiv:0712.0803 [hep-ex]]; Phys. Lett. B **693**, 522 (2010) [arXiv:1006.0618 [hep-ex]].

[3] ATLAS Collaboration, G. Aad *et al.*, Phys. Lett. B **705**, 415 (2011) [arXiv:1107.2381 [hep-ex]]; Phys. Rev. D **85**, 012005 (2012) [arXiv:1108.6308 [hep-ex]].

[4] CMS Collaboration, S. Chatrchyan *et al.*, Phys. Rev. D **85**, 0032002 (2012) [arXiv:1110.4973 [hep-ex]]; CMS Physics Analysis Summary CMS PAS EWK-10-010 (2011) [https://cds.cern.ch/record/1337272]; CMS PAS SMP-12-025 (2013) [https://cds.cern.ch/record/1528579].

[5] P.B. Arnold and M.H. Reno, Nucl. Phys. B **319**, 37 (1989); (E) B **330**, 284 (1990).

[6] R.J. Gonsalves, J. Pawłowski, and C.-F. Wai, Phys. Rev. D **40**, 2245 (1989); Phys. Lett. B **252**, 663 (1990).

[7] N. Kidonakis and V. Del Duca, Phys. Lett. B **480**, 87 (2000) [hep-ph/9911460].

[8] N. Kidonakis and A. Sabio Vera, JHEP **02**, 027 (2004) [hep-ph/0311266].

[9] R.J. Gonsalves, N. Kidonakis, and A. Sabio Vera, Phys. Rev. Lett. **95**, 222001 (2005) [hep-ph/0507317].

[10] N. Kidonakis, in Proceedings of *DIS 2011* [arXiv:1105.4267 [hep-ph]]; in Proceedings of *DPF 2011*, eConf C110809 [arXiv:1109.1578 [hep-ph]].

[11] N. Kidonakis and R.J. Gonsalves, Phys. Rev. D **87**, 014001 (2013) [arXiv:1201.5265 [hep-ph]].

[12] N. Kidonakis and R.J. Gonsalves, in Proceedings of *DPF 2011*, eConf C110809 [arXiv:1109.2817 [hep-ph]]; PoS (ICHEP2012) 051 (2013) [arXiv:1212.2543 [hep-ph]].

[13] T. Becher, C. Lorentzen, and M.D. Schwartz, Phys. Rev. Lett. **108**, 012001 (2012) [arXiv:1106.4310 [hep-ph]].

[14] T. Becher, G. Bell, and S. Marti, JHEP **04**, 034 (2012) [arXiv:1201.5572 [hep-ph]].

[15] T. Becher, C. Lorentzen, and M.D. Schwartz, Phys. Rev. D **86**, 054026 (2012) [arXiv:1206.6115 [hep-ph]].

[16] T. Becher, G. Bell, C. Lorentzen, and S. Marti, JHEP **02**, 004 (2014) [arXiv:1309.3245 [hep-ph]].

[17] A.D. Martin, W.J. Stirling, R.S. Thorne, and G. Watt, Eur. Phys. J. C **63**, 189 (2009) [arXiv:0901.0002 [hep-ph]].